

# Reaching Fermi degeneracy via universal dipolar scattering

K. Aikawa,<sup>1</sup> A. Frisch,<sup>1</sup> M. Mark,<sup>1</sup> S. Baier,<sup>1</sup> R. Grimm,<sup>1,2</sup> and F. Ferlaino<sup>1</sup>

<sup>1</sup>*Institut für Experimentalphysik and Zentrum für Quantenphysik,  
Universität Innsbruck, Technikerstraße 25, 6020 Innsbruck, Austria*

<sup>2</sup>*Institut für Quantenoptik und Quanteninformation, Österreichische Akademie der Wissenschaften, 6020 Innsbruck, Austria  
(Dated: December 19, 2013)*

We report on the creation of a degenerate dipolar Fermi gas of erbium atoms. We force evaporative cooling in a fully spin-polarized sample down to temperatures as low as 0.2 times the Fermi temperature. The strong magnetic dipole-dipole interaction enables elastic collisions between identical fermions even in the zero-energy limit. The measured elastic scattering cross section agrees well with the predictions from dipolar scattering theory, which follow a universal scaling law depending only on the dipole moment and on the atomic mass. Our approach to quantum degeneracy proceeds with very high cooling efficiency and provides large atomic densities, and it may be extended to various dipolar systems.

PACS numbers: 03.75.Ss, 37.10.De, 51.60.+a, 67.85.Lm

Identical fermions with short-range interaction do not collide at very low temperatures [1]. According to the rules of quantum mechanics, the requirement of anti-symmetry of the fermionic wave function causes the scattering cross section to vanish in the ultracold regime. This makes ultracold fermions special in many respects. For instance, they realize perfectly non-interacting quantum systems, which can serve for sensitive interferometers [2] and ultra-precise atomic clocks [3]. From another point of view, the absence of collisions means that direct evaporative cooling cannot work.

The inapplicability of direct evaporative cooling to fermions challenged scientists to develop alternative strategies. The common solution is to use mixtures of two distinguishable atomic components [4]. In this scheme, fermions are sympathetically cooled through elastic *s*-wave collisions with fermions in other spin states [4–8], with atoms belonging to a different isotope [9–13], or with atoms of a different chemical element [14–17].

The scenario is completely different in the presence of the long-range dipole-dipole interaction (DDI). While the effect of the short-range van der Waals interaction still freezes out at low temperatures, as it does for non-dipolar fermions, the DDI prevents the elastic cross section between identical fermions from vanishing. The corresponding Wigner threshold law, governing the threshold behavior of two-body scattering, gives a finite and energy-independent elastic cross section [18–20]. As a key consequence, identical dipolar fermions can collide even in the zero-temperature limit.

Ultracold dipolar scattering is currently attracting a renewed interest in connection with recent experiments on polar molecules [21, 22] and strongly magnetic atoms [13, 23, 24]. Early theoretical work on H atoms and atoms in electric fields suggested that dipolar scattering could provide an elastic cross section that is large enough for direct evaporative cooling of identical fermions [25–28]. Recent theoretical work has elucidated the universal character of the dipolar scattering [29–31] and found that the elastic dipolar cross section is determined only by the mass and the dipole moment of the particles [30]. Recent experiments on fermionic ground-state polar

KRb molecules have tested this prediction and have obtained evidence for the anisotropic character of the DDI [21]. Experiments on using dipolar scattering for evaporative cooling have been reported for fermionic Dy [13] and KRb molecules [32], both reaching temperatures on the order of the Fermi temperature  $T_F$ .

In this Letter, we report on the creation of a quantum degenerate dipolar Fermi gas of  $^{167}\text{Er}$  atoms. We demonstrate a powerful approach in which the underlying cooling mechanism relies solely on dipolar scattering between spin-polarized fermions. We observe a remarkably high cooling efficiency, leading to very dense Fermi gases with typically  $6.4 \times 10^4$  atoms at a temperature of  $T/T_F = 0.2$  and a peak density of  $4 \times 10^{14} \text{ cm}^{-3}$ . Finally, we confirm the prediction of the universal dipolar scattering theory [29, 30] by measuring the Er elastic cross-section in spin-polarized fermions via cross-dimensional thermalization [33]. Our work opens up a conceptually novel pathway to quantum degeneracy in dipolar systems that can be generalized not only to other strongly magnetic atoms but also to ground-state polar molecules, for which the implementation of sympathetic cooling might be difficult.

The strong dipolar character of Er originates from its large magnetic moment  $\mu$  of  $7\mu_B$ , where  $\mu_B$  is the Bohr magneton, and its large mass [20, 34]. Among the six stable isotopes, Er has one fermionic isotope,  $^{167}\text{Er}$ , with a large natural abundance of 23%. While the bosonic isotopes have no hyperfine structure,  $^{167}\text{Er}$  has a nuclear spin  $I = 7/2$ , giving rise to a manifold of eight hyperfine levels and 104 magnetic sub-levels in the electronic ground state [35]. In spite of the much more complex energy structure of the fermionic isotope, our approach to quantum degeneracy is very similar to the one we have successfully used to condense the bosonic isotope  $^{168}\text{Er}$  [24, 36]. It consists of a laser cooling stage followed by direct evaporative cooling in an optical dipole trap (ODT). The fundamental difference with respect to the bosonic case is that the thermalization between spin-polarized fermions proceeds solely through dipolar elastic collisions. In the present work, we focus on spin-polarized fermions in the lowest hyperfine

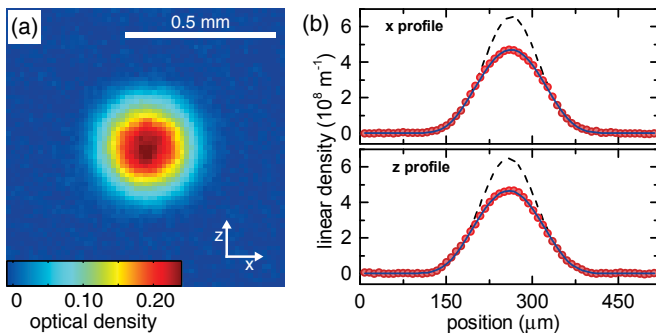


FIG. 1: (color online) Time-of-flight absorption image of a degenerate Fermi gas of Er atoms at  $T/T_F = 0.21(1)$  after  $t_{\text{TOF}} = 12$  ms of expansion (a) and its density distribution integrated along the  $z$  direction (upper panel) and  $x$  direction (lower panel) (b). The observed profiles (circles) are well described by fitting a poly-logarithmic function to the data (solid lines), while they substantially deviate from a fit using a Gaussian distribution to the outer wings of the cloud, i. e.  $w$  (dashed lines). The absorption image is averaged over six individual measurements.

sublevel  $|F = 19/2, m_F = -19/2\rangle$ , where  $F$  is the total spin quantum number and  $m_F$  is its projection along the quantization axis.

Our laser cooling scheme relies on a Zeeman slower operating at 401 nm and on a magneto-optical trap (MOT) based on a narrow line at 583 nm [36]. Both light fields act on transitions with quantum numbers  $F = 19/2 \rightarrow F' = 21/2$ , which are sufficiently closed for laser cooling. In our scheme, fermions in the MOT are naturally spin-polarized into the lowest magnetic sublevel  $|19/2, -19/2\rangle$  because of a combined effect of gravity and the MOT light [36]. We typically capture  $1 \times 10^7$  atoms at  $T = 7 \mu\text{K}$  in the MOT. All measurements in the present work are performed by absorption imaging on the 401-nm transition.

For evaporative cooling, we first transfer the atoms from the MOT into a single-beam large-volume ODT at 1064 nm and then into a tightly focused ODT at 1570 nm. The first trap is used as an intermediate step to increase the transfer efficiency from the MOT. It consists of a single horizontal beam with a power of 20 W and elliptical focus. The beam waists are approximately  $20 \mu\text{m}$  and  $200 \mu\text{m}$  in the vertical and horizontal direction, respectively. The corresponding trap depth is roughly  $100 \mu\text{K}$ . From the large-volume trap, the atoms are loaded into a tightly focused ODT at 1570 nm. This second trap is made of a single horizontal beam, which is collinear to the large-volume trapping beam and has a waist of  $15 \mu\text{m}$ . The initial power of the 1570 nm beam is 1.8 W, corresponding to trap frequencies of  $(\nu_x, \nu_y, \nu_z) = (2147, 51, 2316)$  Hz and a trap depth of about  $k_B \times 190 \mu\text{K}$ . Here,  $z$  is the direction of gravity. At this stage, we have  $1.5 \times 10^6$  atoms at  $T/T_F = 4.4$  with  $T = 28 \mu\text{K}$  and a peak density of about  $1.2 \times 10^{14} \text{ cm}^{-3}$ . The Fermi temperature is defined as  $T_F = h\bar{\nu}(6N)^{1/3}/k_B$ , where  $\bar{\nu}$  is the geometric mean of the trap frequencies and  $h$  is the Planck constant. We force evaporation by reducing the power of the horizontal beam in a near-exponential manner.

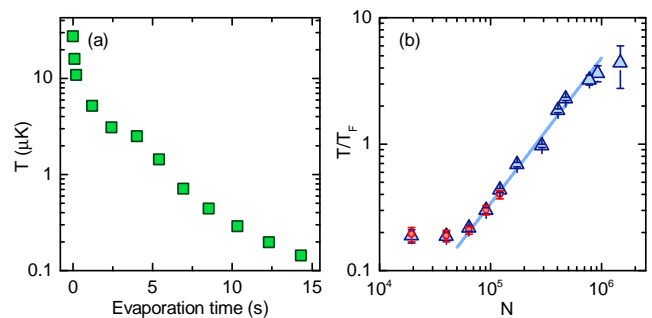


FIG. 2: (color online) Evaporation trajectory to Fermi degeneracy. (a) Temperature evolution during the evaporation ramp and (b) corresponding  $T/T_F$  versus  $N$ . The ratio  $T/T_F$  is obtained from the width  $\sigma$  of the distribution (triangles) and from the fugacity (circles); see text. The error bars originate from statistical uncertainties in temperature, number of atoms, and trap frequencies for the width measurements and the standard deviations obtained from several independent measurements for the fugacity. The solid line is a linear fit to the data for  $0.2 < T/T_F < 4$ .

When  $T_F$  is reached, we introduce a vertical beam at 1570 nm to confine the fermions into the crossed region created by the two beams and to preserve the atomic density. Its power is gradually increased and reaches 1.2 W at the end of the evaporation. The vertical beam has a beam waist of  $33 \mu\text{m}$ . During evaporation, we apply a homogeneous guiding magnetic field to maintain the spin-polarization in the system. At high temperature, the magnetic field value is about 1.7 G, which is large enough to avoid any thermal excitation into higher spin states. For temperature below  $3.2T_F$ , we decrease the value of the magnetic field to 0.59 G, where we observe a slightly better evaporation efficiency. After 10 s of forced evaporation, we obtain a deeply degenerate Fermi gas.

Figure 1(a) shows a typical time-of-flight (TOF) absorption image of a degenerate dipolar Fermi gas of  $N = 6.4 \times 10^4$  and a peak density of  $n_0 = 4 \times 10^{14} \text{ cm}^{-3}$  at  $T/T_F = 0.21(1)$  with  $T_F = 1.33(2) \mu\text{K}$ . At this point, our trap frequencies are (470, 346, 345) Hz. Fermi degeneracy reveals itself in a smooth change of the momentum distribution from a Maxwell-Boltzmann to a Fermi-Dirac distribution [37]. Correspondingly, the atomic density profile is expected to change its Gaussian shape into a poly-logarithmic one. A fit to TOF images reveals that at temperatures above  $\approx 0.5T_F$  the Gaussian and poly-logarithmic function are hardly distinguishable from each other and both describe the data well. By further decreasing the temperature, we observe a gradually increasing deviation from the Gaussian shape. This deviation is evident in Fig. 1(b), which shows a density profile at  $T/T_F = 0.21(1)$ . A Gaussian fit to the outer wings of the cloud, i. e. outside the disk with radius  $w$ , with  $w$  being the  $1/e$  diameter of the Gaussian fit to the entire cloud, clearly overestimates the population at the center of the cloud. This is a fingerprint of Fermi degeneracy, meaning that the population of low-energy levels is limited by the Pauli exclusion principle.

In all our measurements, we extract  $T/T_F$  from fits to the

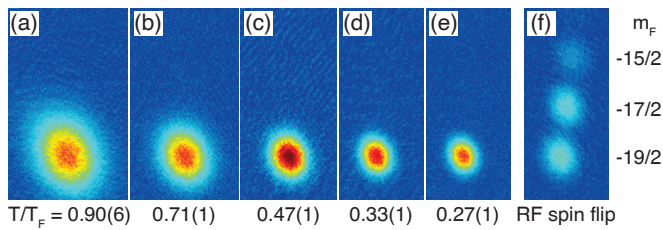


FIG. 3: (color online) Absorption images of the atomic cloud with a Stern-Gerlach separation of the spin components. A magnetic field gradient of about 40 G/cm is applied during the expansion for about 7 ms. (a)-(e) Along the entire evaporative cooling sequence, atoms are always spin-polarized in the lowest hyperfine sublevel  $|F = 19/2, m_F = -19/2\rangle$ .  $T/T_F$  of the atomic samples are indicated in each panel. In (f) the image is obtained right after RF mixing of the spin states for the sample at  $T/T_F = 0.33(1)$ . The three clouds correspond to the magnetic sublevels  $m_F = -19/2$ ,  $-17/2$ , and  $-15/2$  from bottom to top.

density profiles using either a poly-logarithmic or a Gaussian function. In the former case, the fit gives both the fugacity  $\zeta$  and the parameter  $\sigma$  characterizing the width of the distribution. The fugacity directly gives  $T/T_F = [-6 \times \text{Li}_3(-\zeta)]^{-1/3}$ , with  $\text{Li}_n$  being the  $n$ -th order poly-logarithmic function [7, 9]. The parameter  $\sigma$  is related to the atomic temperature by  $T = m\sigma^2 / (k_B t_{\text{TOF}}^2)$ , where  $t_{\text{TOF}}$  is the time of flight and  $m$  is the mass of  $^{167}\text{Er}$ , and together with  $T_F$ , calculated from  $N$  and  $\bar{v}$ , gives a more indirect value for  $T/T_F$ . We determine  $T/T_F$  using both methods, which show well consistent results.

To get deeper insights into the evaporation process and the underlying collisional properties we study the evaporation trajectory. Figure 2 summarizes our results. We observe that the evaporation first proceeds with high efficiency down to temperatures well below  $T_F$  and then plateaus at about  $T/T_F = 0.2$ . The latter behavior suggests that further cooling is limited by Pauli blocking [4, 6, 7, 9] and that more thoroughly optimized evaporation ramps might be needed to reach even lower temperatures. The deepest degeneracy we attained is  $T/T_F = 0.19(1)$  with  $N = 4.0 \times 10^4$ . From the slope of the evaporation trajectory, we obtain the efficiency parameter  $\gamma$ . This parameter quantifies the gain in phase-space density PSD at the expense of the atom number and can be written as  $\gamma = -d(\ln \text{PSD})/d(\ln N) = -3 \times d(\ln T/T_F)/d(\ln N)$ . From a linear fit to the data down to  $T/T_F = 0.2$ , we find  $\gamma = 3.5(2)$ . This remarkably large number is in the league of the best evaporation efficiencies observed in experiments with ultracold atoms based on  $s$ -wave scattering, including our experiments with the bosonic  $^{168}\text{Er}$  [24] and experiments on strongly interacting two-component Fermi gases [5, 38, 39].

Our interpretation of the cooling process in terms of dipolar scattering relies on the full spin polarization of the sample. Another spin state being present would lead to  $s$ -wave collisions in the sample. Therefore it is important to make sure that we do not have any other spin state present. For this reason, we carry out a dedicated set of Stern-Gerlach-type measurements at various stages of the evaporation. During the

whole evaporation sequence, we never observe any population in spin states different from the  $m_F = -19/2$  state. Figure 3(a-e) shows the relevant portion of the TOF image, where atoms are observed. To identify unambiguously the spatial positions of the different spin components, we intentionally prepare a spin mixture by radio-frequency (RF) transfer; see Fig. 3(f). It is worth to mention that we observe fast spin relaxation when a multi-component mixture is prepared [40].

The effectiveness of our evaporative cooling scheme suggests a very favorable ratio of the elastic scattering rate to the inelastic one. We explore elastic scattering by measuring the elastic dipolar cross section  $\sigma_{\text{el}}$  in our spin-polarized fermionic sample via cross-dimensional thermalization experiments [33]. We compress the system in one spatial direction by increasing the power of the vertical beam by about a factor of three. We then monitor the time evolution of the temperature in the other direction, as shown in the inset of Fig. 4. The time constant  $\tau$  for cross-dimensional thermalization is directly connected to  $\sigma_{\text{el}}$  through the relation  $\tau = \alpha / (\bar{n} \sigma_{\text{el}} v)$ , where  $\alpha$  is the number of collisions required to thermalize,  $\bar{n}$  is the mean density, and  $v = 4\sqrt{k_B T / (\pi m)}$  is the mean relative velocity. A delicate point of our analysis is the estimation of  $\alpha$ , which depends on the underlying scattering mechanism. We employ  $\alpha = 4.1$ , which has been numerically calculated for non-dipolar  $p$ -wave collisions and has been applied to KRb polar molecules [21]. Although  $p$ -wave collisions are expected to be the leading term in dipolar scattering of identical fermions, more detailed calculations of  $\alpha$  might be needed to fully account for the mixing of partial waves resulting from the DDI [41].

In this way, we explore elastic scattering over a wide range of atom numbers from  $3 \times 10^4$  to  $1.1 \times 10^5$  and for various final temperatures ranging from 300 to 600 nK. Our findings at 0.59 G [42] are shown in Fig. 4. In the non-degenerate regime ( $T \gtrsim T_F$ ), we obtain a constant elastic cross section with a mean value of  $2.0(5) \times 10^{-12} \text{cm}^2$ , corresponding to  $[2.7(3) \times 10^2 a_0]^2$ , where  $a_0$  is the Bohr radius. The error bar is mainly due to systematic uncertainties in trap frequencies, temperature, and number of atoms. Below  $T_F$ , the effect of quantum degeneracy becomes visible through a suppression of scattering events caused by Pauli blocking. In this regime, we can interpret our measurements in terms of an effective elastic cross section, which also includes the Pauli suppression factor. As expected, we observe a substantial decrease of the effective  $\sigma_{\text{el}}$  for decreasing  $T/T_F$ , similarly to the case of  $s$ -wave collisions between fermions in different spin states [44].

Dipolar scattering theories predict an energy-independent elastic cross section for identical fermions in the low-energy regime [18–20]. The cross section is predicted to follow a universal scaling law that is fully determined by a single parameter - the dipolar length  $D$  [30] - and it reads as

$$\sigma_{\text{el}} = 6.702 \times D^2, \quad (1)$$

where  $D = 2\pi^2 d^2 m / h^2$  with  $d^2 = \mu_0 \mu^2 / (4\pi)$  and  $\mu_0$  being the vacuum permeability. This equation shows a clear analogy to the ordinary  $s$ -wave scattering, where  $D$  plays the role

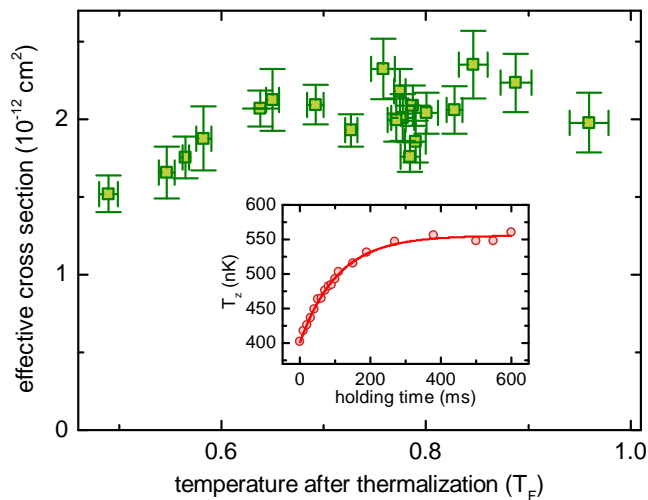


FIG. 4: (color online) Effective elastic cross-section as a function of  $T/T_F$  after thermalization. In the non-degenerate regime, the effective cross section is constant and gives a mean value of  $2.0(5) \times 10^{-12} \text{cm}^2$ . The error bars for each point contain the statistical uncertainties of the time constant for cross-dimensional thermalization, of the trap frequencies, and of the temperature. A typical cross-dimensional thermalization measurement with an exponential fit to the data is shown in the inset.  $T_z$  is the temperature along the  $z$ -direction.

of the scattering length. For the Er parameters, the universal theory predicts  $\sigma_{\text{el}} = 1.8 \times 10^{-12} \text{cm}^2$ , which is in reasonable agreement with the measured value. The small deviation might be due to the chosen value for  $\alpha$ , to systematic errors, or to a residual effect of the short-range physics, which is not included in the theory.

Our observations suggest that inelastic losses are very weak. Since the atoms are fully polarized in the lowest spin state, inelastic losses can only be caused by collisions with the background gas and by three-body decay. To investigate this more quantitatively, we carry out atom-decay measurements by recording the number of atoms as a function of the hold time in an ODT initially loaded with  $N \simeq 1 \times 10^5$  atoms at  $T/T_F \simeq 0.47$ . In spite of the very high peak density of  $3 \times 10^{14} \text{cm}^{-3}$ , we find the atom number to decay in a purely exponential manner (time constant 40s) without showing any signature of three-body processes. From this observation we can derive an upper limit for the three-body recombination rate constant as low as  $L_3 \leq 3 \times 10^{-30} \text{cm}^6/\text{s}$ .

The remarkable efficiency of evaporative cooling in a single-component Fermi gas of Er and the exceptionally high densities together with low inelastic collision rates can be understood in terms of a very favorable combination of the DDI with the  $p$ -wave barrier. While DDI is strong enough to provide us with a sufficient cross section for elastic collisions, it is weak enough to preserve a substantial repulsive barrier for any alignment of the colliding dipoles. Even for the case of maximum dipolar attraction (head to tail configuration), the effective potential, given by the interplay between the  $p$ -

wave barrier and the DDI, features a repulsive barrier with a maximum height  $V(r_{\text{max}}) = 2\hbar^2/(27mD^2)$  at  $r_{\text{max}} = 3D$ . For Er, the barrier height still exceeds  $k_B \times 7 \mu\text{K}$ , which is much larger than all collision energies in the final evaporation stage. This prevents atoms from getting close to each other and three-body decay, which requires short-range interactions, is strongly suppressed.

In conclusion, we produce a degenerate dipolar Fermi gas of  $^{167}\text{Er}$  atoms. We demonstrate direct evaporative cooling of identical fermions via universal dipolar scattering. Our method provides two key advantages: feeble inelastic losses and exceptionally high attainable densities. The former aspect is favorable for reaching low values of  $T/T_F$ , which are ultimately limited by the so-called hole-heating mechanism caused by inelastic losses [45, 46]. The latter aspect has important consequences for dipolar physics. The relevant energy scale for dipolar phenomena at the many-body level is given by  $n_0 d^2$  [20, 34]. Given the high densities achieved here, our degenerate Fermi gas of Er currently is the most dipolar quantum gas available in experiments, with  $n_0 d^2$  being 0.92% of the Fermi energy. We speculate that even much higher densities than the ones here attained may be achieved since we do not see any limiting process. This may open a way for observing  $p$ -wave pairing in dipolar gases and for the creation of an anisotropic Fermi superfluid [47, 48].

We are grateful to J. Bohn, C. Salomon, M. Baranov, and M. Zwierlein for fruitful discussions. We thank M. Springer for technical support and NKT Photonics for lending us the 1570 nm fiber laser. This work is supported by the Austrian Ministry of Science and Research (BMWF) and the Austrian Science Fund (FWF) through a START grant under Project No. Y479-N20 and by the European Research Council under Project No. 259435. K. A. is supported within the Lise-Meitner program of the FWF.

- 
- [1] S. Giorgini, L. P. Pitaevskii, and S. Stringari, *Rev. Mod. Phys.* **80**, 1215 (2008).
  - [2] G. Roati, E. de Mirandes, F. Ferlaino, H. Ott, G. Modugno, and M. Inguscio, *Phys. Rev. Lett.* **92**, 230402 (2004).
  - [3] T. Nicholson, M. Martin, J. Williams, B. Bloom, M. Bishof, M. Swallows, S. Campbell, and J. Ye, *Phys. Rev. Lett.* **109**, 230801 (2012).
  - [4] B. DeMarco and D. S. Jin, *Science* **285**, 1703 (1999).
  - [5] S. R. Granade, M. E. Gehm, K. M. O'Hara, and J. E. Thomas, *Phys. Rev. Lett.* **88**, 120405 (2002).
  - [6] T. Fukuhara, Y. Takasu, M. Kumakura, and Y. Takahashi, *Phys. Rev. Lett.* **98**, 030401 (2007).
  - [7] B. DeSalvo, M. Yan, P. Mickelson, Y. M. De Escobar, and T. Killian, *Phys. Rev. Lett.* **105**, 030402 (2010).
  - [8] S. Taie, Y. Takasu, S. Sugawa, R. Yamazaki, T. Tsujimoto, R. Murakami, and Y. Takahashi, *Phys. Rev. Lett.* **105**, 190401 (2010).
  - [9] M. K. Tey, S. Stellmer, R. Grimm, and F. Schreck, *Phys. Rev. A* **82**, 011608 (2010).
  - [10] A. G. Truscott, K. E. Strecker, W. I. McAlexander, G. B. Partridge, and R. G. Hulet, *Science* **291**, 2570 (2001).

- [11] F. Schreck, L. Khaykovich, K. L. Corwin, G. Ferrari, T. Bourdel, J. Cubizolles, and C. Salomon, *Phys. Rev. Lett.* **87**, 080403 (2001).
- [12] J. M. McNamara, T. Jelten, A. S. Tychkov, W. Hogervorst, and W. Vassen, *Phys. Rev. Lett.* **97**, 080404 (2006).
- [13] M. Lu, N. Q. Burdick, and B. L. Lev, *Phys. Rev. Lett.* **108**, 215301 (2012).
- [14] G. Roati, F. Riboli, G. Modugno, and M. Inguscio, *Phys. Rev. Lett.* **89**, 150403 (2002).
- [15] Z. Hadzibabic, C. A. Stan, K. Dieckmann, S. Gupta, M. W. Zwierlein, A. Gorlitz, and W. Ketterle, *Phys. Rev. Lett.* **88**, 160401 (2002).
- [16] C. Silber, S. Gunther, C. Marzok, B. Deh, P. W. Courteille, and C. Zimmermann, *Phys. Rev. Lett.* **95**, 170408 (2005).
- [17] F. M. Spiegelhalter, A. Trenkwalder, D. Naik, G. Hendl, F. Schreck, and R. Grimm, *Phys. Rev. Lett.* **103**, 223203 (2009).
- [18] L. D. Landau and E. M. Lifshitz, *Quantum Mechanics, vol. 3 (Course of theoretical physics)* (Butterworth-Heinemann, Oxford, 1977).
- [19] H. Sadeghpour, J. Bohn, M. Cavagnero, B. Esry, I. Fabrikant, J. Macek, and A. Rau, *J. Phys. B* **33**, R93 (2000).
- [20] M. A. Baranov, *Phys. Rep.* **464**, 71 (2008).
- [21] K. K. Ni, S. Ospelkaus, D. Wang, G. Quemener, B. Neyenhuis, M. H. G. de Miranda, J. L. Bohn, J. Ye, and D. S. Jin, *Nature* **464**, 1324 (2010).
- [22] M. H. G. de Miranda, A. Chotia, B. Neyenhuis, D. Wang, G. Quémener, S. Ospelkaus, J. L. Bohn, J. Ye, and D. S. Jin, *Nature Physics* **7**, 502 (2011).
- [23] M. Lu, N. Q. Burdick, S. H. Youn, and B. L. Lev, *Phys. Rev. Lett.* **107**, 190401 (2011).
- [24] K. Aikawa, A. Frisch, M. Mark, S. Baier, A. Rietzler, R. Grimm, and F. Ferlaino, *Phys. Rev. Lett.* **108**, 210401 (2012).
- [25] J. M. V. A. Koelman, H. T. C. Stoof, B. J. Verhaar, and J. T. M. Walraven, *Phys. Rev. Lett.* **59**, 676 (1987).
- [26] J. M. V. A. Koelman, H. T. C. Stoof, B. J. Verhaar, and J. T. M. Walraven, *Phys. Rev. B* **38**, 9319 (1988).
- [27] M. Marinescu and L. You, *Phys. Rev. Lett.* **81**, 4596 (1998).
- [28] W. Geist, A. Idrizbegovic, M. Marinescu, T. Kennedy, and L. You, *Phys. Rev. A* **61**, 013406 (1999).
- [29] C. Ticknor, *Phys. Rev. Lett.* **100**, 133202 (2008).
- [30] J. L. Bohn, M. Cavagnero, and C. Ticknor, *New J. Phys.* **11**, 055039 (2009).
- [31] Z. Idziaszek and P. S. Julienne, *Phys. Rev. Lett.* **104**, 113202 (2010).
- [32] J. Ye, private communication (2013).
- [33] C. R. Monroe, E. A. Cornell, C. A. Sackett, C. J. Myatt, and C. E. Wieman, *Phys. Rev. Lett.* **70**, 414 (1993).
- [34] M. A. Baranov, M. Dalmonte, G. Pupillo, and P. Zoller, *Chem. Rev.* **112**, 5012 (2012).
- [35] A. Frisch, K. Aikawa, M. Mark, F. Ferlaino, E. Berseneva, and S. Kotochigova, *Phys. Rev. A* **88**, 032508 (2013).
- [36] A. Frisch, K. Aikawa, M. Mark, A. Rietzler, J. Schindler, E. Zupanic, R. Grimm, and F. Ferlaino, *Phys. Rev. A* **85**, 051401 (2012).
- [37] M. Inguscio, W. Ketterle, and C. Salomon, eds., *Ultra-cold Fermi Gases* (IOS Press, Amsterdam, 2008), Proceedings of the International School of Physics “Enrico Fermi”, Course CLXIV, Varenna, 20-30 June 2006.
- [38] M. Bartenstein, A. Altmeyer, S. Riedl, S. Jochim, C. Chin, J. Hecker Denschlag, and R. Grimm, *Phys. Rev. Lett.* **92**, 120401 (2004).
- [39] M. W. Zwierlein, C. A. Stan, C. H. Schunck, S. M. F. Raupach, A. J. Kerman, and W. Ketterle, *Phys. Rev. Lett.* **92**, 120403 (2004).
- [40] K. Aikawa, A. Frisch, M. Mark, S. Baier, R. Grimm, and F. Ferlaino, in preparation (2013).
- [41] J. Bohn and D. Jin, private communication (2013).
- [42] The magnetic fields are chosen to avoid Er Feshbach resonances [43].
- [43] A. Frisch, M. Mark, K. Aikawa, F. Ferlaino, J. L. Bohn, C. Makrides, A. Petrov, and S. Kotochigova, arXiv: 1312.1972 (2013).
- [44] B. DeMarco, S. B. Papp, and D. S. Jin, *Phys. Rev. Lett.* **86**, 5409 (2001).
- [45] E. Timmermans, *Phys. Rev. Lett.* **87**, 240403 (2001).
- [46] L. D. Carr, T. Bourdel, and Y. Castin, *Phys. Rev. A* **69**, 033603 (2004).
- [47] L. You and M. Marinescu, *Phys. Rev. A* **60**, 2324 (1999).
- [48] M. A. Baranov, M. S. Mar’enko, V. S. Rychkov, and G. V. Shlyapnikov, *Phys. Rev. A* **66**, 013606 (2002).